Wideband extinction measurements for thin and planar samples

Larsson, Christer; Sohl, Christian; Gustafsson, Mats; Kristensson, Gerhard

2008

CODEN:LUTEDX/(TEAT-7166)/1-10/(2008)

Wideband extinction measurements for thin and planar samples

Christer Larsson, Christian Sohl, Mats Gustafsson, and Gerhard Kristensson

Electromagnetic Theory
Department of Electrical and Information Technology
Lund University
Sweden

Christer Larsson, Christian Sohl, Mats Gustafsson, and Gerhard Kristensson
{Christer.Larsson,Christian.Sohl,Mats.Gustafsson,Gerhard.Kristensson}@eit.lth.se

Department of Electrical and Information Technology
Electromagnetic Theory
P.O. Box 118
SE-221 00 Lund
Sweden

Editor: Gerhard Kristensson

Abstract

A method to determine the extinction cross section for a thin and planar object for a large bandwidth in the microwave region is developed. The method is based on a regular measurement of the monostatic radar cross section. It is compared to and validated with a more general measurement method based on a measurement of the radar cross section in the forward direction. The result shows that monostatic RCS measurements can be used with good accuracy to determine the extinction cross section for this type of thin samples.

1 Introduction

This paper describes a method to determine the extinction cross section and the extinction volume for a thin and non-magnetic planar object over a large bandwidth in the microwave region. The method is based on a conventional measurement of the monostatic radar cross section (RCS). The method is compared to and validated with a more general measurement method that is based on a measurement of the RCS in the forward direction. The experiments are performed on a fabricated single-layer planar 33×33 array of quadratic split ring resonators (SRR) tuned for resonance at 8 GHz.

The motivation to measure the extinction cross section, *i.e.*, the sum of the total scattering cross section and the absorption cross section, comes from the need to verify theoretical results that bound the scattering from objects. These results that have the form of general summation rules for the extinction cross section are derived in Refs. 16, 17 and 18. Through the optical theorem it is possible to calculate the extinction cross section from the forward RCS, see Refs. 11 and 12.

A large majority of radar applications are monostatic *i.e.*, the transmitting and receiving antennas are colocated. Bistatic systems are used for some applications, see Ref. 21, but are more complicated than monostatic systems due to the requirement to synchronize the received signal with the transmitted. This becomes especially difficult if the one or both of the transmitter and the receiver are moving. There are some applications where improved functionality due to the bistatic geometry provides an offset to the increased system complexity, *e.g.*, counter stealth. Systems that utilize the scattering in the forward direction (scattering at 180° bistatic angle) have some special applications, such as ground target identification, see Ref. 2 or radar fences, see Ref. 21, but are not common. Most free space scattering measurements at indoor or outdoor measurement ranges are therefore performed in a monostatic geometry. As a consequence, there are relatively few studies published that treat the free space measurement of forward scattering at microwave frequencies.

A bistatic measurement system described in the open literature where forward scattering can be measured in the laboratory is described in Refs. 3 and 4. It operates in the 2–12.4 GHz range with a measurement accuracy of ± 1 dB at a level of -18 dBsm for the forward RCS. This should be compared to the results for monostatic RCS at the same measurement range where it is possible to measure

down to -50 dBsm with this accuracy.

In comparison, there is a wealth of literature treating monostatic RCSn measurements, see *e.g.*, Refs. 5 and 10. There are also standardized procedures for monostatic measurements, see Ref. 8. Monostatic measurements are therefore, from a practical point of view, to be preferred if they can be used for the purpose at hand.

The direct measurement of the forward RCS in free space is experimentally difficult since the largest part of the received field at the receiving antenna consists of direct illumination by the transmitting antenna. The direct illumination contributes with a dominating background that has to be removed, with signal processing or otherwise, from the scattered field component that one wants to determine.

The purpose of this paper is to develop and validate a method to determine the extinction cross section for thin and planar samples from monostatic RCS measurements.

2 Theory

This section gives a short theoretical background to the general summation rules that bound the scattering from objects and defines the quantities that we want to determine through measurements.

In a series of papers in Refs. 16, 17 and 18, the use of a forward dispersion relation is exploited by utilizing the optical theorem. It is established in these papers that the extinction cross section integrated over all frequencies is related to the static polarizability dyadics of the scatterer. This interesting result has many application, *e.g.*, one area with large potential is antennas, see Refs. 6 and 7. In this section we define the most important quantities in the theory using RCS notation.

Consider the direct scattering of a plane electromagnetic wave $\boldsymbol{E}_0 \mathrm{e}^{-\mathrm{i}2\pi \hat{\boldsymbol{k}}\cdot\boldsymbol{r} f/\mathrm{c}_0}$ with time dependence $\mathrm{e}^{-\mathrm{i}2\pi f t}$ impinging in the $\hat{\boldsymbol{k}}$-direction on a bounded scatterer surrounded by free space (c_0 is the phase velocity of light in free space). The material of the scatterer is modeled by linear constitutive relations which satisfy primitive causality, passivity, and are independent of time, *i.e.*, no material aging.

The scattering properties in the $\hat{\boldsymbol{r}}$-direction are described for the incident wave polarization $\hat{\boldsymbol{e}}_\mathrm{i} = \boldsymbol{E}_0/|\boldsymbol{E}_0|$, polarization of the scattered wave $\hat{\boldsymbol{e}}_\mathrm{s} = \boldsymbol{E}_\mathrm{s}(\boldsymbol{r})/|\boldsymbol{E}_\mathrm{s}(\boldsymbol{r})|$ and polarization of the received wave $\hat{\boldsymbol{e}}_\mathrm{r}$. The partial bistatic RCS amplitude that is recorded in a measurement is then defined as,

$$A(\hat{\boldsymbol{r}}, \hat{\boldsymbol{e}}_\mathrm{r}) = \frac{2\sqrt{\pi}}{|\boldsymbol{E}_0|} \lim_{r\to\infty} \mathrm{e}^{-\mathrm{i}2\pi f r/\mathrm{c}_0} r \boldsymbol{E}_\mathrm{s}(\boldsymbol{r}) \cdot \hat{\boldsymbol{e}}_\mathrm{r}, \tag{2.1}$$

The complex quantity A preserves the phase information present in the measurement, $r = |\boldsymbol{r}|$ denotes the magnitude of the position vector $\boldsymbol{r}$. The maximum amplitude can then be written,

$$A_\mathrm{max}(\hat{\boldsymbol{r}}) = \max_{\hat{\boldsymbol{e}}_\mathrm{r}\cdot\hat{\boldsymbol{k}}=0} |A(\hat{\boldsymbol{r}}, \hat{\boldsymbol{e}}_\mathrm{r})| = |A(\hat{\boldsymbol{r}}, \hat{\boldsymbol{e}}_\mathrm{s})| = \frac{2\sqrt{\pi}}{|\boldsymbol{E}_0|} \lim_{r\to\infty} r|\boldsymbol{E}_\mathrm{s}(\boldsymbol{r})| \tag{2.2}$$

The partial bistatic RCS, *i.e.*, the bistatic RCS measured with receiver antenna polarization $\hat{\boldsymbol{e}}_{\mathrm{r}}$, can then be defined as,

$$\sigma(\hat{\boldsymbol{r}},\hat{\boldsymbol{e}}_{\mathrm{r}}) = |A(\hat{\boldsymbol{r}},\hat{\boldsymbol{e}}_{\mathrm{r}})|^2 = \lim_{r\to\infty} \frac{4\pi}{|\boldsymbol{E}_0|^2} r^2 |\boldsymbol{E}_{\mathrm{s}}(\boldsymbol{r})\cdot\hat{\boldsymbol{e}}_{\mathrm{r}}|^2 \tag{2.3}$$

In particular, (2.3) evaluated in the backward direction $\hat{\boldsymbol{r}} = -\hat{\boldsymbol{k}}$ yields the well-known monostatic RCS in Ref. 10. The partial bistatic RCS in (2.3) has its maximum when the polarization of the receiving antenna matches the polarization of the scattered wave. The maximum bistatic RCS is then,

$$\sigma_{\max}(\hat{\boldsymbol{r}}) = \max_{\hat{\boldsymbol{e}}_{\mathrm{r}}\cdot\hat{\boldsymbol{k}}=0} \sigma(\hat{\boldsymbol{r}},\hat{\boldsymbol{e}}_{\mathrm{r}}) = |A_{\max}(\hat{\boldsymbol{r}})|^2 = \frac{4\pi}{|\boldsymbol{E}_0|^2} \lim_{r\to\infty} r^2 |\boldsymbol{E}_{\mathrm{s}}(\boldsymbol{r})|^2 \tag{2.4}$$

The scattering cross section σ_{s} is defined as the total scattered power in all directions divided by the incident power flux. It is obtained by integrating (2.4) over the unit sphere with respect to $\hat{\boldsymbol{r}}$, see Ref. 14.

$$\sigma_{\mathrm{s}} = \frac{1}{4\pi} \iint \sigma_{\max}(\hat{\boldsymbol{r}})\,\mathrm{dS} = \frac{1}{|\boldsymbol{E}_0|^2} \lim_{r\to\infty} r^2 \iint |\boldsymbol{E}_{\mathrm{s}}(\boldsymbol{r})|^2\,\mathrm{dS} \tag{2.5}$$

Here, $\mathrm{dS} = \sin\theta\,\mathrm{d}\theta\,\mathrm{d}\phi$ denotes the differential solid angle in terms of the polar and azimuthal variables $\theta \in [0,\pi]$ and $\phi \in [0,2\pi)$, respectively. Based on (2.5), the extinction cross section $\sigma_{\mathrm{ext}} = \sigma_{\mathrm{s}} + \sigma_{\mathrm{a}}$ is defined as the sum of the scattering and absorption cross sections, where the latter is a measure of the absorbed power in the scatterer, see Ref 1. The extinction cross section can also be determined from the forward RCS via the optical theorem

$$\sigma_{\mathrm{ext}} = \frac{2\mathrm{c}_0}{|\boldsymbol{E}_0| f} \lim_{r\to\infty} r\,\mathrm{Im}\left\{ \mathrm{e}^{-\mathrm{i}2\pi f r/\mathrm{c}_0} \hat{\boldsymbol{e}}_{\mathrm{i}}^* \cdot \boldsymbol{E}_{\mathrm{s}}(r\hat{\boldsymbol{k}}) \right\} = \frac{\mathrm{c}_0}{\sqrt{\pi} f}\,\mathrm{Im}\, A(\hat{\boldsymbol{k}},\hat{\boldsymbol{e}}_{\mathrm{i}}^*), \tag{2.6}$$

where * denotes the complex conjugate.

A dispersion relation for the combined effect of scattering and absorption of electromagnetic waves is derived in Ref. 17 from the holomorphic properties of the forward scattering dyadic. The result is a summation rule for the extinction cross section valid for any linear and non aging scatterer obeying passivity and primitive causality. Defining the extinction volume

$$\varrho = \frac{\mathrm{c}_0^2}{8\pi^{5/2} f^2} A(\hat{\boldsymbol{k}},\hat{\boldsymbol{e}}_{\mathrm{i}}^*), \tag{2.7}$$

where ϱ and σ_{ext} are related by,

$$\frac{8\pi^2 f}{\mathrm{c}_0}\,\mathrm{Im}\,\varrho = \sigma_{\mathrm{ext}}. \tag{2.8}$$

From the integral representations in Ref. 20 or the discussion on page 11 of Ref. 14, it follows that for a planar and infinitely thin scatterer subject to a wave

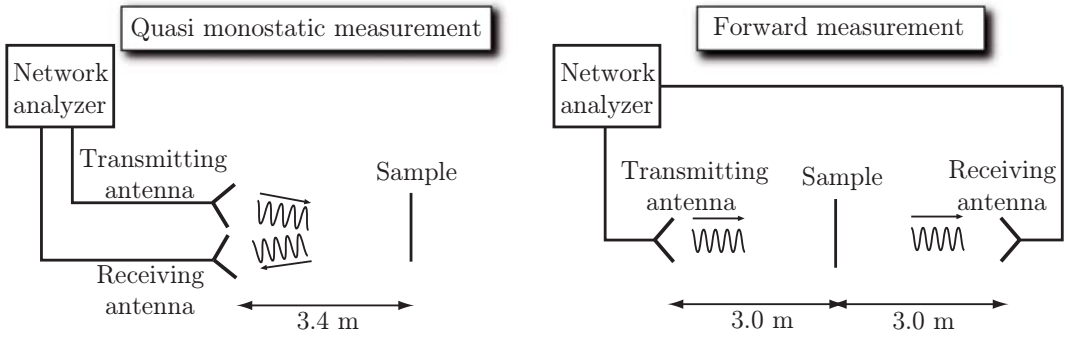

Figure 1: The setups for quasi monostatic and forward RCS measurements

incident at normal incidence, the partial bistatic RCS in the backward and forward directions are identical *i.e.*,

$$A(-\hat{\boldsymbol{k}}, \hat{\boldsymbol{e}}_{\mathrm{r}}) = A(\hat{\boldsymbol{k}}, \hat{\boldsymbol{e}}_{\mathrm{r}}). \tag{2.9}$$

Combining the two equations (2.6) and (2.9) and noting that $\hat{\boldsymbol{e}}_{\mathrm{i}} = \hat{\boldsymbol{e}}_{\mathrm{i}}^{*}$ for linear polarization makes it possible to determine the extinction cross section by a measurement of the partial monostatic RCS amplitude. Using this in (2.6) and (2.7) gives σ_{ext} and ϱ.

3 Experimental setup

In Ref. 13 it is suggested that an array of split ring resonators can be used to obtain a negative magnetic permeability material. The fabricated sample used in this study is designed as a single-layer planar array of quadratic split ring resonators (SRR) tuned for resonance at 8 GHz. The design is similar to the square split ring resonator array used in Ref. 15. It consists of 33×33 unit cells supported by a square FR4 substrate of edge length 140 mm and thickness 0.3 mm, see Fig. 2. The relative dielectric constant, ϵ_{rel}, of the substrate varies between 4.2 and 4.4 in the measured frequency interval, with an overall dielectric loss tangent less than $4.8 \cdot 10^{-3}$.

3.1 Monostatic RCS measurements

Monostatic RCS measurements are performed in an anechoic chamber. The sample is mounted on an expanded polystyrene sample (EPS) holder placed on a pylon. The chamber is set up for quasi monostatic RCS measurements with two dual polarized ridged circular waveguide horns positioned at a distance of 3.55 m from the sample, see Fig. 1. The measurement uses an Agilent Performance Network Analyzer (PNA) transmitting a continuous wave without online hard or software gating. The polarization of the transmitted and received waves is horizontal with respect

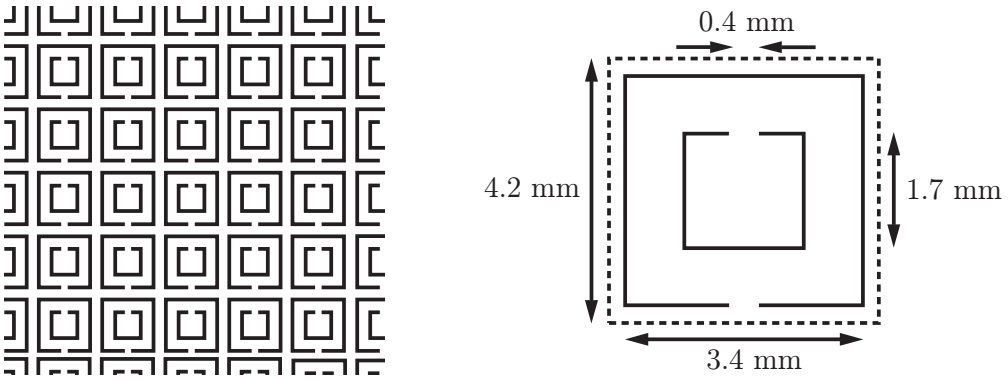

Figure 2: A section of the printed pattern of the fabricated sample (left figure) and the geometry of the square unit cell (right figure). The line width of the printed circuit is 0.1 mm.

to the pattern in Fig. 2. The original frequency interval $[2, 20]$ GHz is reduced to $[3.2, 19.5]$ GHz due to range (time) domain filtering of the data. The latter frequency interval is sampled with 7246 equidistant points corresponding to an unambiguous range of 66.7 m, or 445 ns. This is sufficient to avoid influence of room reverberations.

Calibration including both amplitude and phase is performed using a metal plate with the same outer dimensions as the sample. A physical optics expression for a perfectly conducting plate is used as calibration reference, see page 523 in Ref. 14. In order to validate the calibration method we also perform a Method of Moments calculation for the metal plate. The results from this calculation do not deviate significantly from the physical optics result. The metal plate is, in addition to being used for calibration, also used to align the experimental setup using the metal plate specular reflection.

The data from the measurements are processed by a coherent subtraction of the background followed by a calibration using the physical optics approximation. The frequency domain data is then transformed to the range domain, where the response from the sample is selected from the range profile using a 1.1 m spatial gate. Finally, the selected data is transformed back to the frequency domain.

The background subtraction combined with the time gating is sufficient to suppress the background by 15–25 dB. This gives a background level of better than -50 dBsm for the frequency range above 5 GHz and -40 dBsm to -30 dBsm for the lowest part of the frequency range. The high background level at the lower frequencies is due to that the wideband horns illuminate the walls at these frequencies. This background can be maintained subtracting with only one background measurement obtained in the beginning or at the end of the day.

3.2 Forward RCS measurements

Forward RCS measurements are performed using a different setup with ridged waveguide horns in an ordinary lab area. The fabricated sample is mounted on an ex-

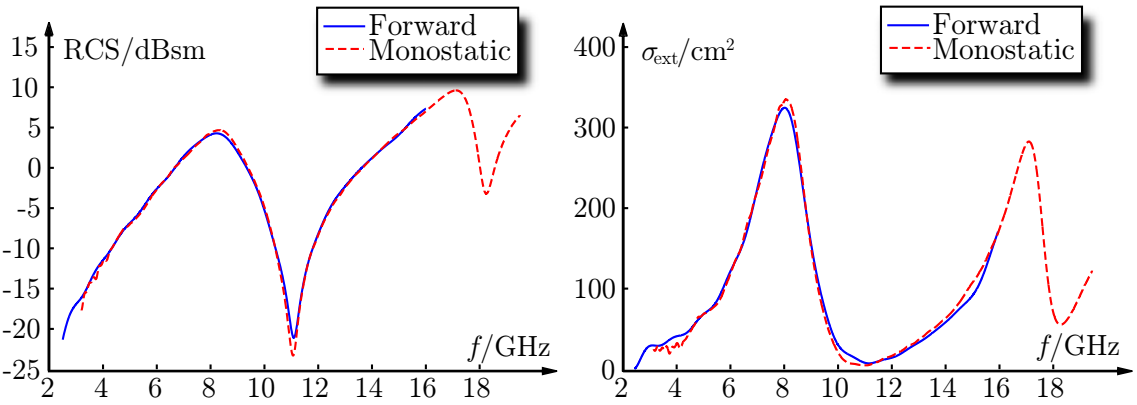

Figure 3: Measured monostatic and forward RCS (left figure) and extinction cross section (right figure). The curve corresponding to the extinction cross section calculated from the forward measurement is adjusted corresponding to a path length difference delay of 3.4 ps.

panded polystyrene sample holder placed on an EPS column. The antennas are positioned facing each other at a distance of 6.00 m with the sample at the midpoint between the antennas, see Fig. 1. In this case an HP 8720C Network Analyzer is used for the measurements with a similar waveform as for the monostatic measurements. The instrument is limited to only 1601 frequency points for one frequency sweep so four sweeps are interlaced in order to obtain 6404 frequency points. The original frequency interval $[1, 18]$ GHz is reduced to $[2.5, 16]$ GHz due to time domain filtering of the data. The latter frequency interval is sampled with 5086 equidistant points corresponding to an unambiguous time of 378 ns. Here we use time units as a measure for the ambiguity since a range in distance units is less meaningful for forward scattering. This is sufficient to avoid influence of room reverberations such as delayed scattering from the floor and the walls.

Calibration including both amplitude and phase is performed using a sphere with radius 6 cm. The Mie series for a perfectly conducting sphere is used as calibration reference, see Ref. 14. A sphere is an ideal forward scattering calibration object since there are no alignment problems that would arise with other objects, see Ref. 4.

The calibration measurement is done by first measuring the calibration sphere followed by a measurement of the background. The raw data from the calibration measurement is then processed by coherent subtraction of the background. The Mie series result is divided by the background subtracted calibration data to obtain the calibration vector. The sample is aligned and measured, and also in this case, followed by a measurement of the background that is coherently subtracted from the sample measurement. The repeated background measurements are needed in order to increase the efficiency of the background subtraction and to obtain the background levels mentioned below. We perform the background measurement within less than 2 minutes after each sample (calibration) measurement.

The background subtracted sample data is then calibrated using the calibration

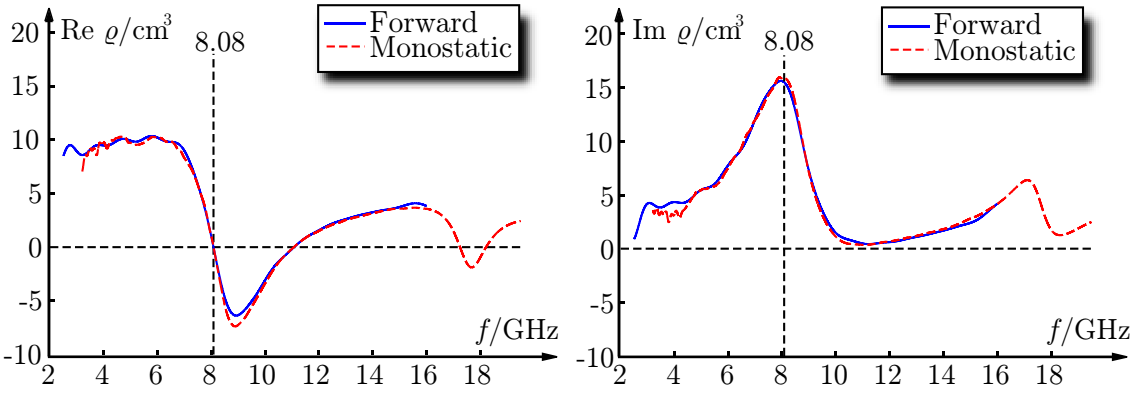

Figure 4: Comparison of the real (left) and imaginary (right) parts of the extinction volume ϱ obtained from the monostatic and forward scattering measurements, respectively. The forward scattering curves are adjusted corresponding to a path length difference delay of 3.4 ps.

vector. The calibrated frequency domain data is transformed to the time domain, where the response from the sample is selected from the time profile using a 0.25 m spatial gate. The size of the gate was chosen so that the contribution from the background was minimized. Finally, the selected data is transformed back to the frequency domain. The background subtraction combined with the time gating is sufficient to suppress the background by 50 dB giving a background level of less than −40 dB.

4 Results and discussion

The result from the monostatic RCS measurements are compared with the results from the forward scattering experiments in this section. The monostatic and forwards scatter RCS from the sample are compared in Fig. 3. The agreement is is very good as can be seen. The only significant differences are the 0.4 dBsm difference for the maxima at 8.1 GHz and the 2.4 dBsm difference for the minima at 11.1 GHz. It should be pointed out that Fig. 3 shows the measured data after calibration and time gating without other normalization or adjustment. The extinction cross section data, σ_{ext} are obtained from the RCS using (2.6), see Fig. 3. The maxima differ only 3% (or 0.14 dB) in this case. The extinction cross section obtained from the forward scattering experiment was adjusted with a frequency dependent phase shift corresponding to a 3.4 ps delay according to the procedure described below. The real and imaginary part of ϱ are obtained from the RCS using (2.7), see Fig. 4. The phase of the extinction volume obtained from the forward scattering experiment was adjusted corresponding to a delay of 3.4 ps. The adjustment was performed by matching the value of the zero crossing of the real component of ϱ obtained from the forward scattering measurement with the zero crossing obtained of the real component of ϱ from the monostatic measurement. We believe that the

largest contribution to this phase shift is the delay the wave experiences as it passes the 0.3 mm thick FR4 substrate and the 48 mm EPS sample support. It is possible to estimate the dielectric constant, ϵ, from the density of EPS using Ref. 9. From a density of 18.4 mg/cm^3 we get $\epsilon_{\text{rel}} = 1.02$ for the EPS sample holder. This gives a relative delay of 1.7 ps. Using $\epsilon_{\text{rel}} = 4.3$ gives a relative delay of 1.1 ps for the FR4 substrate adding up to a total relative delay of 2.8 ps. Small alignment differences between the calibration plate and the sample can also account for some of the phase difference. As a reference, 1 ps corresponds to a 0.15 mm offset between the calibration plate and the sample. Validation experiments were also performed for the negative permittivity sample in Ref. 19 with similar results.

The results in Figs. 3 and 4 show that the assumption of symmetry between monostatic RCS measurements and forward scattering measurements is, see (2.9), correct within experimental accuracy for these samples. This means that monostatic measurement can be used to determine the extinction cross section for thin and planar samples. However, for other samples, forward scattering experiments are the only practical way to obtain the extinction cross section. We are currently developing and refining the methods for forward scattering measurements to be able to measure a more general class of samples.

5 Conclusions

It is shown that monostatic RCS measurements can be used to determine the extinction cross section and the extinction volume for thin samples by validating with a forward RCS measurement. The differences in measured phase can be explained by different path lengths in the two measurements and the differences in amplitude are well within experimental error limits. The method employing forward scattering to determine the extinction cross section is currently being developed. With this it will be possible to determine the extinction cross section for more general objects. This work will be reported in forthcoming papers.

Acknowledgments

The financial support by the Swedish Research Council is gratefully acknowledged. The authors also thank Saab Bofors Dynamics, Linköping, Sweden, and in particular Carl-Gustaf Svensson and Mats Andersson for generous hospitality and practical assistance with the monostatic measurements.

References

[1] C. F. Bohren and D. R. Huffman. *Absorption and Scattering of Light by Small Particles.* John Wiley & Sons, New York, 1983.

[2] M. Cherniakov, R. Abdullah, P. Jancovic, M. Salous, and V. Chapursky. Automatic ground target classification using forward scattering radar. *IEE Proceedings Radar, Sonar and Navigation*, **153**(5), 427–437, 2006.

[3] M. G. Cote. Automated swept-angle bistatic scattering measurements using continuous wave radar. *IEEE Trans. Instrumentation and Measurement*, **41**(2), 185–192, 1992.

[4] M. G. Cote. Automated swept-angle bistatic measurement system. Technical Report RL-TR-93-52, Rome Laboratory, Rome Laboratory/ERCT, 31 Grenier Street, Hansom AFB MA 01731-3010, 1993. http://stinet.dtic.mil.

[5] N. C. Curry. *Techniques of radar reflectivity measurement.* Artech House, Dedham, 1984.

[6] M. Gustafsson, C. Sohl, and G. Kristensson. Physical limitations on antennas of arbitrary shape. *Proc. R. Soc. A*, **463**, 2589–2607, 2007.

[7] M. Gustafsson, C. Sohl, and G. Kristensson. Physical limitations on antennas of arbitrary shape. Technical Report LUTEDX/(TEAT-7153)/1–37/(2007), Lund University, Department of Electrical and Information Technology, P.O. Box 118, S-221 00 Lund, Sweden, 2007. http://www.eit.lth.se.

[8] IEEE recommended practice for radar cross-section test procedures, 2007. IEEE Std 1502-2007.

[9] E. F. Knott. Dielectric constant of plastic foams. *IEEE Trans. Antennas Propagat.*, **41**(8), 1167–1171, 1993.

[10] E. F. Knott, J. F. Shaeffer, and M. T. Tuley. *Radar Cross Section.* SciTech Publishing Inc., 5601 N. Hawthorne Way, Raleigh, NC 27613, 2004.

[11] R. Newton. Optical theorem and beyond. *Am. J. Phys*, **44**, 639–642, 1976.

[12] R. G. Newton. *Scattering Theory of Waves and Particles.* Dover Publications, New York, second edition, 2002.

[13] J. B. Pendry, A. J. Holden, D. J. Robbins, and W. J. Stewart. Magnetism from conductors and enhanced nonlinear phenomena. *IEEE Trans. Microwave Theory Tech.*, **47**(11), 2075–2084, 1999.

[14] G. T. Ruck, D. E. Barrick, W. D. Stuart, and C. K. Krichbaum. *Radar Cross-Section Handbook*, volume 1 and 2. Plenum Press, New York, 1970.

[15] D. R. Smith, S. Schultz, P. Markos, and C. M. Soukoulis. Determination of effective permittivity and permeability of metamaterials from reflection and transmission coefficients. *Phys. Rev. B*, **65**, 195104–195108, 2002.

[16] C. Sohl, M. Gustafsson, and G. Kristensson. The integrated extinction for broadband scattering of acoustic waves. *J. Acoust. Soc. Am.*, **122**(6), 3206–3210, 2007.

[17] C. Sohl, M. Gustafsson, and G. Kristensson. Physical limitations on broadband scattering by heterogeneous obstacles. *J. Phys. A: Math. Theor.*, **40**, 11165–11182, 2007.

[18] C. Sohl, M. Gustafsson, and G. Kristensson. Physical limitations on metamaterials: Restrictions on scattering and absorption over a frequency interval. *J. Phys. D: Applied Phys.*, **40**, 7146–7151, 2007.

[19] C. Sohl, C. Larsson, M. Gustafsson, and G. Kristensson. A scattering and absorption identity for metamaterials: experimental results and comparison with theory. Submitted for publication in J. Appl. Phys., 2007.

[20] S. Ström. Introduction to integral representations and integral equations for time-harmonic acoustic, electromagnetic and elastodynamic wave fields. In V. V. Varadan, A. Lakhtakia, and V. K. Varadan, editors, *Field Representations and Introduction to Scattering*, volume 1 of *Handbook on Acoustic, Electromagnetic and Elastic Wave Scattering*, chapter 2, pages 37–141. Elsevier Science Publishers, Amsterdam, 1991.

[21] N. J. Willis. *Bistatic Radar*. Artech House, Boston, London, 1991.